Int. J. Electrochem. Sci., 14 **(2019)** 3805 – 3823, doi: 10.20964/2019.04.35

International Journal of ELECTROCHEMICAL SCIENCE
www.electrochemsci.org

Electrocatalytic Reduction of CO_2 on Mono-Metal/Graphene/Polyurethane Sponge Electrodes

Yajing Yang[1], *Linyuan Wang*[1], *Xin Ma*[1], *Liangsheng Zhu*[2], *Zhaoyong Bian*[1,*]

[1] College of Water Sciences, Beijing Normal University, Beijing 100875, PR China
[2] College of Environmental Science and Engineering, Beijing Forestry University, Beijing 100083, PR China
[*]E-mail: bian@bnu.edu.cn

Received: 28 November 2018 / *Accepted:* 8 January 2019 / *Published:* 10 March 2019

Metal nanoparticle (Pd, Cu, Fe, Ru and In)/graphene nanostructure catalysts for the electrocatalytic reduction of CO_2 have been prepared by sodium borohydride ($NaBH_4$) reduction. The nanostructure catalysts were characterized by X-ray diffraction (XRD), scanning electron microscopy (SEM), transmission electron microscopy (TEM), X-ray photoelectron spectroscopy (XPS), and cyclic voltammetry (CV). Moreover, a strategy to fabricate metal/graphene/polyurethane sponge (MGS) for the reduction of CO_2 through a facile and inexpensive 'dipping and drying' method was studied. The MGS electrode was characterized by SEM and linear sweep voltammetry (LSV) scans. Metal nanoparticles (Pd, Cu, Fe, Ru and In) with average sizes of 5.9, 5.4, 4.3, 6.2 and 4.2 nm were uniformly dispersed on the surface of graphene sheets with a noncrystalline structure. Metal/graphene nanostructure catalysts were well covered on the polyurethane sponge. When the voltage was less than the peak potential, sharper increases of the reduction current under CO_2 were observed, and the peak potentials (Pd, Cu, Fe, Ru and In) were −1.21, −1.25, −1.36, −1.38 and −1.10 V, which provided evidence for the catalytic reduction of CO_2 by the metal/graphene catalysts and the peak potential of 1% In/graphene was the smallest. However, the peak potential order of MGS was consistent with the metal/graphene catalysts, basically 1% In/graphene (−0.58 V) < 1% Cu/graphene (−0.71 V) < 1% Pd/graphene (−0.78 V) < 1% Ru/graphene (−0.80 V) <1% Fe/graphene (−1.1 V). Therefore, the MGS electrode, as a supporting skeleton for metal/graphene catalysts, not only exhibits similar electrochemical properties of the metal/graphene catalysts, but also inherits the nature of the polyurethane sponge as a support material. Hence, the good performance of MGS makes it a promising candidate electrode for the electrocatalytic reduction of CO_2.

Keywords: electrocatalytic reduction; CO_2; polyurethane sponge; metal/graphene catalyst; gas diffusion electrode

1. INTRODUCTION

In the past few decades, the dramatic increase in atmospheric CO_2 has caused global warming and other severe environmental issues [1, 2]. However, the need for non-renewable fossil fuels has prioritized the environmental problems [3]. The best approach to address the two issues is to reduce the release of CO_2 and convert this to hydrocarbon fuels [4, 5]. Different approaches have been used to convert CO_2, such as chemical, photochemical reduction and electrochemical reduction [6, 7]. Therefore, the electrocatalytic process has been widely studied because of its unique advantages [8]. High over-potential and low selectivity are two key issues for the electrochemical reduction of CO_2, which mainly depends on the material and metal used [9, 10]. Various metal-based catalysts (such as Cu, Pt, Fe, In, Au, Sn and Pd) have been used to improve the energy efficiency of the electrochemical reduction of CO_2 [11, 12]. Cu, Fe, In, Ru, and Pd are considered as promising metals for the reduction of CO_2. The hydrogen evolution potential (HER) of In is very high and the main reduced product is HCOOH [13, 14]. The Pd electrode presents a low hydrogen over-potential, and CO and HCOOH have been reported as the main products at a low over-potential [15]. Economic and high activity have meant that non-noble metals, such as Fe and Cu, have also been widely studied [16, 17].

However, the mass transport limitations have resulted in the selectivity and current efficiencies remaining low, because of the low solubility of CO_2 [18, 19]. Gas diffusion electrodes (GDEs) on which are nanostructure carbon materials catalysts, such as carbon black, carbon nanotubes and graphene, have been used [20-22]. Graphene has been widely used as an electrode material or catalyst in an electrochemical reaction to promote electron transfer, because of its excellent electrical conductivity, chemical stability, high mechanical strength, and properties similar to a metal or semiconductor [23, 24]. The unique electronic and physical properties of graphene improve the reaction kinetics of noble metal nanoparticles and enhance the CO_2 reduction kinetics [25]. In addition to the characteristics discussed above, the large special surface area and high chemical stability make graphene more suitable as catalyst supports [25]. Furthermore, a large number of reactive groups, such as hydroxyl groups on graphene surface, can provide sites for metal loading [26]. The carbon vacancies in graphene can be used as anchoring points for the growth of metal nanoparticles. These two important features will increase the durability of the metal-graphene system and prevent sintering of the metal nanoparticles [27].

CO_2 can easily be transferred to the electrodes and distributed well over the surfaces of a catalyst even at a low current density [28]. However, the cumbersome preparation methods for GDEs require a large amount of catalyst, so it would not be suitable for large-scale industrial applications [29]. New simple and practical preparation methods of GDEs have to be researched. A super-capacitor electrode fabricated by graphene/MnO_2 nano-structured sponge allows good accessibility of the electrolyte to hybrid electrode materials [30]. Novel sponge super-capacitors fabricated by a simple “dipping and drying” method have resulted in good conductivity and full accessibility of the electrolyte to the electrode, and have dramatically improved the performance of super-capacitors [31]. Additionally, a graphene-sponge (polyurethane sponge)-stainless steel composite electrode has been used as an anode for microbial fuel cells. The composite electrode, fabricated by the ‘dipping and drying’ process, clearly holds great promise for field applications with high-performance, low-cost, and highly conductive nature [32].

In this work, metal/graphene catalysts have been prepared and characterized by X-ray diffraction (XRD), scanning electron microscopy (SEM), transmission electron microscopy (TEM), and X-ray photoelectron spectroscopy (XPS). Polyurethane sponge was eventually chosen as a skeleton to support the metal/graphene catalyst. A new strategy to fabricate a metal/graphene/polyurethane sponge electrode (MGS) for the reduction of CO_2 through a facile and inexpensive dip coating method has been demonstrated. SEM has been used to observe the distribution of metal/graphene on the surface of the sponge. The electrochemical performance of metal/graphene catalysts and MGS were investigated by cyclic voltammetry (CV) and linear sweep voltammetry (LSV) scans, respectively.

2. EXPERIMENTAL

2.1 Preparation of metal/graphene catalysts

Graphite oxides (GO) were synthesized from graphite powder (Guo Yao Co., Ltd., Beijing, China) in accordance with the modified Hummers' method [33, 34]. GO (100 mg) was dispersed in deionized water (100 mL) and ultrasonicated for 2 h (1.0 mg/mL). A different metal precursor was then added into the GO aqueous solution. The metal precursors were $PdCl_2$, $Cu(CH_3COO)_2 \cdot H_2O$, $FeCl_3 \cdot 6H_2O$, $RuCl_3$ and $In_2(SO_4)_3$. After vigorous stirring for 10 min, the pH of the mixture solution was adjusted to 10.0 by adding $NH_3 \cdot H_2O$, and then stirred for 2 h. The pH of deionized water (40 mL) was also adjusted to 10.0. $NaBH_4$ (1 g) was slowly dissolved into the deionized water (pH = 10) in an ice-water bath. Our research group has already studied the electro-catalytic reduction of CO_2 by wt% Pd/graphene and wt% Cu/graphene catalysts, and found that when the Pd and Cu contents were 1%, the reduction effect was optimized [35]. Therefore, the metal loading of this experiment was 1%. For the 1% Pd/graphene, 1% Cu/graphene, and 1% Fe/graphene catalysts, the reduction process was as follows. $NaBH_4$ solution was added into the GO aqueous dispersions drop-by-drop in an ice-water bath and then stirred for 12 h at 25 ^oC. After completion of the reaction, the product was washed with a large amount of deionized water and suction filtered; the resulting sample was dried in a vacuum oven at 60 ^oC for 12 h. For the 1% In/graphene and 1% Ru/graphene catalysts, the reduction reaction was performed at 80 ^oC for 4 h.

2.2 Preparation of MGS electrodes

The polyurethane and melamine sponge were cut into blocks (1 cm × 1 cm × 0.2 cm) and ultrasonically cleaned in ethanol and distilled water for 3 h. Two sponges were then dried in a vacuum oven at 100 ^oC for 3 h to completely remove the moisture. Three experiments were performed. In the first group, 1% Pd/graphene catalyst (50 mg) was dissolved to deionized water (10 mL), followed by the addition of sodium cholate (5 mg) [32]. In the second group, sodium cholate was replaced by sodium dodecyl benzene sulfonate. In the third group, the solvent was replaced with ethanol (10 mL) without a surfactant. The three solutions were ultrasonicated for 15 min. The as-dried sponge was then dipped into the solutions, and finally dried in the vacuum oven at 90 ^oC for 5 h. The 'dipping-and-drying' process

was repeated in triplicate to increase the 1% Pd/graphene catalysts loading. Then, the 1% Pd/graphene/polyurethane sponge (PGS) electrode was prepared by sandwiching stainless-steel mesh between two pieces of the PGS composite. Then, 1% Cu/graphene, 1% Fe/graphene, and 1% In/graphene catalysts were loaded on the polyurethane sponge by the method which had the best load effect.

2.3. Material characterization

The metal/graphene catalyst was characterized by a Rigaku D/max-III X-ray power diffractometer (X' Pert PRO MPD, Holland) using Cu Kα radiation (λ = 1.5406 nm) with a Ni filter. S-4800 scanning electron microscopy (Hitachi, S-4800, Tokyo, Japan), with a magnification of ×50,000 and emission voltages of 10 kV and 5 kV, was used to determine the particle size, distribution of loaded metal, morphology and the coverage of the metal/graphene catalyst on the sponge. In addition, a transmission electron microscope JEM-2010F (JEOL Co., Ltd., Japan) operated at 200 kV was also used to observe the morphology of metal/graphene catalyst. The surface composition of the metal/graphene catalyst, content of metal and valence state on the surface of graphene were then investigated by an X-ray photoelectron spectrometer (PHI5300, American) using the monochromatic Al Kα line.

2.4 Electrochemical measurements

The electrochemical properties of the metal/graphene catalysts and the MGS electrode were characterized by CV and LSV, respectively, on an electrochemical workstation (CHI660D, Chen Hua Instruments Co., Ltd., Shanghai, China). A three-electrode system was employed. When a glassy carbon (GC) electrode was used as the working electrode, the counter electrode was a platinum wire and an Ag|AgCl electrode (with 3 mol/L KCl) was used as reference electrode. The GC electrode was polished with 1, 0.3, and 0.05 μm Al_2O_3 powder and rinsed by ethanol and deionized water, then dried under an infrared lamp. The metal/graphene catalyst (1.0 mg) was dispersed in 5 wt.% Nafion solution (5 μL) and of 99.5 wt.% ethanol (1 mL) using a high power ultrasonicator for 30 min to form a dispersed solution. A portion of the resulting graphene dispersion (10 μL) was measured and then placed on the GC electrode. Finally, the graphene suspension was coated on the electrode, which was dried by infrared irradiation. The reduction of CO_2 was investigated in $KHCO_3$ (0.5 mol/L) under a scan rate of 200 mV/s with a scanning voltage of 0 to −2 V (vs. Ag|AgCl). The polyurethane sponge with the best loading effect was selected from the several groups, and then used for the MGS electrode. When the MGS electrode was used as the working electrode, the counter electrode was a platinum plate electrode and an Ag|AgCl electrode (with 3 mol/L KCl) was used as the reference electrode. Then LSV was used to study the electrochemical properties of the MGS electrode in 0.5 mol/L $KHCO_3$ under scan rates of 50 mV/s, 100 mV/s, and 200 mV/s. The scanning voltage was 0 to −1.4 V (vs. Ag|AgCl), CO_2 or N_2 was bubbled into the electrolyte for 30 min before electrochemical measurements. To eliminate the effect caused by different pH on the experimental results, HCl was used to adjust the pH, when N_2 was bubbled into the electrolyte. A schematic of the experimental setup is shown in **Fig. 1**.

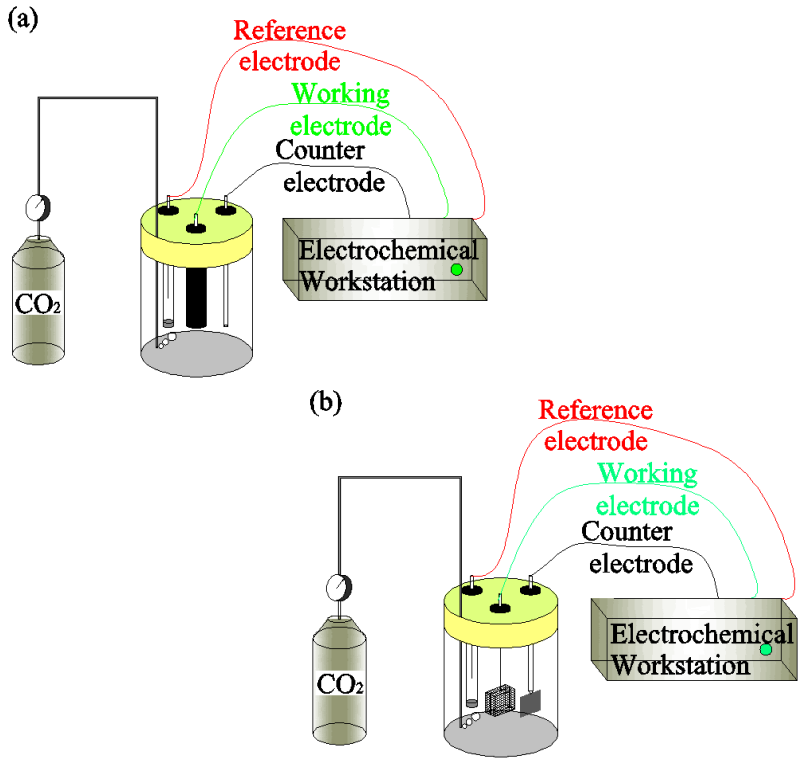

Figure 1. Electrochemical performance testing apparatus for (a) metal/graphene catalyst and (b) MGS electrode.

3. RESULTS AND DISCUSSION

3.1 Characterization of metal/graphene catalysts

To investigate the metal nanoparticle morphology and the dispersion on the graphene, SEM was used for all prepared metal nanoparticle/graphene catalysts. All the SEM images are shown in **Fig. 2**. The white spots in the SEM of metal/graphene were metal particles. From the SEM of 1% Pd/graphene 1% Cu/graphene, and 1% Ru/graphene catalysts, Pd, Cu, and Ru nanoparticles were uniformly dispersed on graphene. In the In/graphene and Fe/graphene catalyst samples, the metal nanoparticles were well dispersed on graphene with less observed particle spots on the surface.

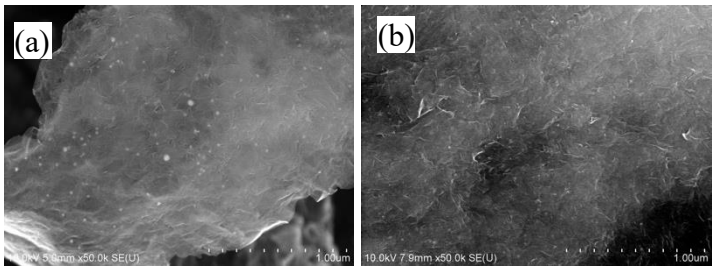

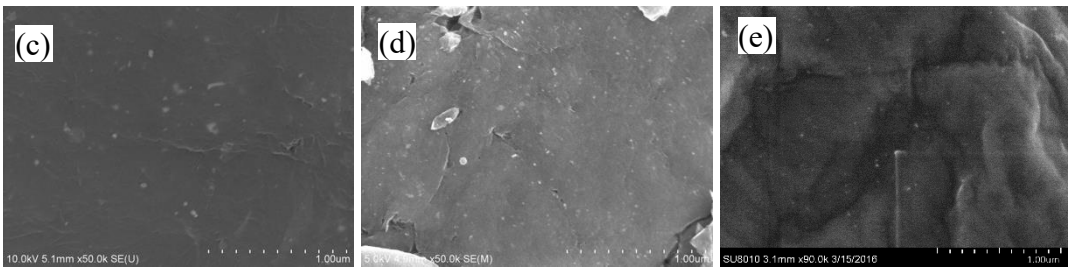

Figure 2. SEM image of (a) 1%Pd/graphene, (b) 1%Cu/graphene, (c) 1%Fe/graphene, (d) 1%In/ graphene, and (e) 1%Ru/ graphene catalyst.

Further distribution of the metal particles on the graphene surface, and the particle size distribution of metal particles could be observed from the TEM of metal/graphene catalysts **(Fig. 3)**. The average particle sizes of the metals in all catalysts were calculated by the normal analysis of the particle size distribution and are listed in **Table 1**. As shown in the TEM image of 1% Pd/graphene catalyst, the black spots, namely Pd particles, were dispersed on the surface of graphene, and the particle size of Pd (6.03±1.14 nm) was larger than other metals (Cu, Fe and In), but smaller than Ru. In accordance with the TEM image of the 1% Cu/graphene catalyst, Cu particles were dispersed well on graphene and the particle size of Cu was 5.28±0.43 nm.

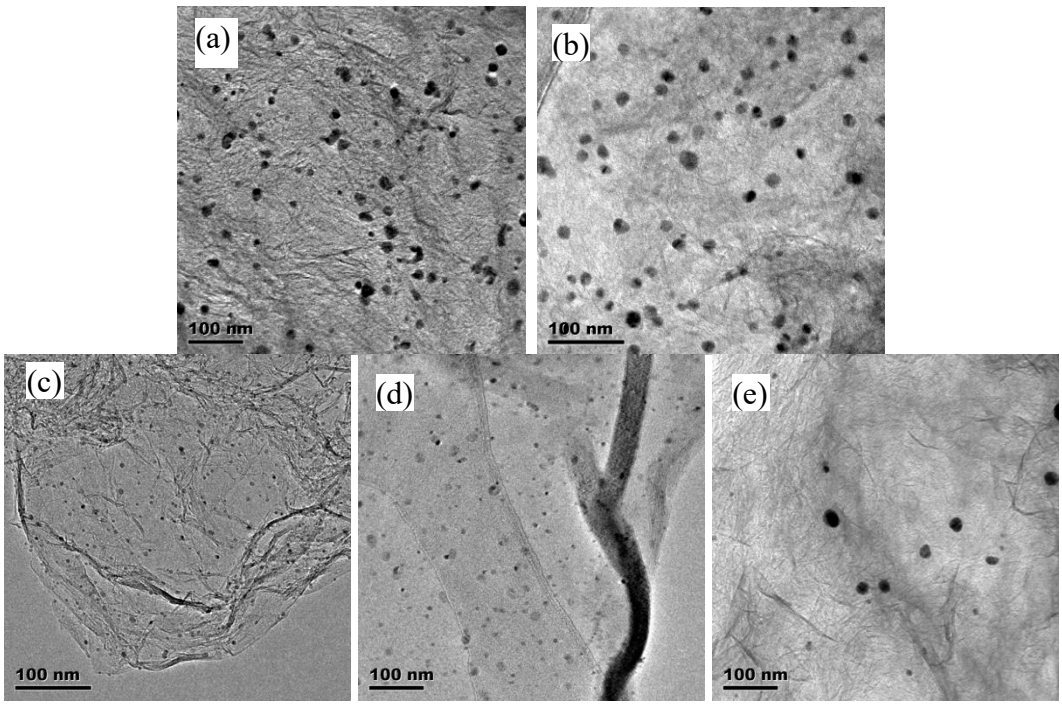

Figure 3. TEM image of (a) 1%Pd/graphene, (b) 1%Cu/graphene, (c) 1%Fe/graphene, (d) 1%In/graphene, and (e) 1%Ru/graphene catalysts.

There was no aggregation of Cu on graphene. In **Table 1**, the particle size of Fe and In were 4.11±0.96 nm and 4.31±0.92 nm, respectively. Hence, the range of the Pd particle size was the biggest, metal In and Fe were second, and the particle size of Cu was the smallest. When the metal particle size is small with a large distribution, it will show excellent catalytic activity.

Table 1. Average particle size of metals calculated by XRD patterns (Scherrer formula) and TEM data in metal/graphene catalysts and the electrochemical characterization data of metal/graphene catalysts and MGS electrodes.

Metal/graphene catalyst	Current of MGS at -1.4 V/mA	Average particle size/nm		Peak potential/V	
		XRD	TEM	Metal/graphene	MGS
1%Pd/graphene	-49.1	5.9	6.03±1.14	-1.21	-0.78
1%Cu/graphene	-18.1	5.2	5.28±0.43	-1.25	-0.71
1%Fe/graphene	-37.5	4.6	4.11±0.96	-1.36	-1.1
1%In/graphene	-27.5	4.9	4.31±0.92	-1.1	-0.58
1%Ru/graphene	-29.1	6.2	6.22±0.88	-1.38	-0.8

The XRD pattern of the metal/graphene catalyst is shown in **Fig. 4**. The diffraction peak at 2θ = 10° in graphite oxide was replaced by the peak appearing at 2θ = 25.5°, which corresponded to the graphite (002) structure appearing in all metal/graphene catalysts. This indicated that most of the oxygen-containing functional groups on GO had been successfully removed and the layer spacing of graphite had become smaller [36]. The diffraction peak at 2θ = 39.9°, which corresponded to Pd (111) in the 1% Pd/graphene catalyst, Cu (111) at 2θ = 43° in the 1% Cu/graphene catalyst, Fe (110) at 2θ = 43.5° in the 1% Fe/graphene catalyst, In (400) at 2θ = 33° in the 1% In/graphene catalyst, and Ru (101) at 2θ = 43.9° in the 1% Ru/graphene indicated that all metals had been successfully loaded onto the graphene surface and reduced to form metal nanoparticles [23, 37-39]. The diffraction peaks from the loaded metal were broad and an obvious crystal structure could not be assigned based on the XRD data. This implied that the Pd, Cu, Fe, In and Ru particles in metal/graphene were amorphous. This also showed that the metal particles were relatively small and dispersed on the carrier uniformly. When the particle crystal size was larger, the characteristic peak would be narrower. The steepness trend of the metal diffraction peaks could be obtained as 1% Fe/graphene < 1% In/graphene < 1% Cu/graphene < 1% Pd/graphene < 1% Ru/graphene. Therefore, it could be inferred that the size of the metal particles was in the order of 1% Fe/graphene < 1% In/graphene < 1% Cu/graphene < 1% Pd/graphene < 1% Ru/graphene. This was consistent with the SEM and TEM characterization results. Metal particle sizes were calculated by the Scherrer formula as shown in **Table 1**.

To analyze the elemental composition and oxidation state of the metal/graphene catalyst, XPS was performed and the results are shown in **Fig. 5**. The prepared catalysts mainly contained C, metal, and O elements according to the survey XPS spectra of all the metal/graphene catalysts**.** The corresponding content of the metal elements in 1% Fe/graphene, 1% In/graphene, 1% Cu/graphene, 1% Pd/graphene, and 1% Ru/graphene catalysts according to XPS were 0.959%, 0.981%, 0.913%, 0.853%, and 0.99%. As shown in the C1s spectrum of the metal/graphene catalysts, three peaks at 284.6, 285.8, and 288.7 eV were observed, which were associated with the sp^2 carbon (C=C/C-C), carbonyl (C-O), and carboxyl (O-C=O) functional groups, respectively. The relative content of sp^2 carbons in the 1% Pd/graphene, 1% Cu/graphene, 1% Fe/graphene, 1% In/graphene and 1% Ru/graphene catalysts were estimated to be 60.1%, 65.5%, 65.8%, 67.1%, and 66.7%, which were much higher than 41.9% in GO

[35]. This indicated that the reduction of GO was not complete and some remaining oxygen of the functional groups had not been removed.

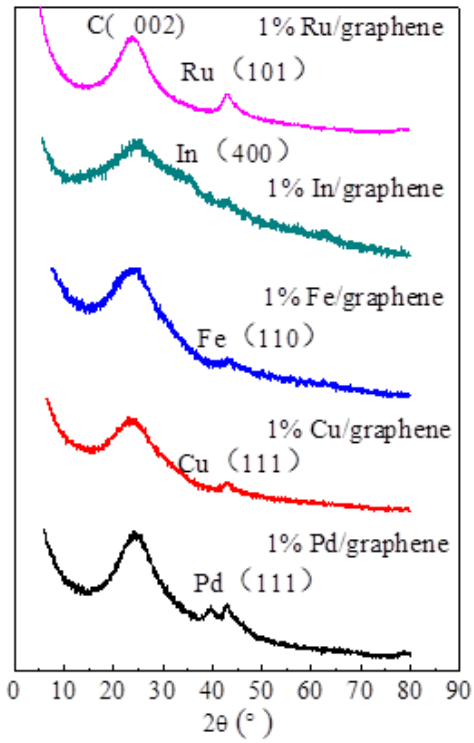

Figure 4. XRD patterns of 1%Pd/graphene, 1%Cu/graphene, 1%Fe/graphene, 1%In/graphene, and 1%Ru/graphene catalysts.

The remaining oxygen-containing functional groups not only gave the graphene samples a hydrophilic feature, but also provided some binding sites for loaded metal nanoparticles [26]. Hence, suitable contents of remaining oxygen functional groups and sp^2 carbons favored the construction of the metal/graphene. The XPS spectrum of the 1% Pd/graphene catalyst (**Fig. 5f**) showed that the electron binding energy emerging at 335 eV and 340.2 eV could be assigned to $Pd^{(0)}$3d5/2 and $Pd^{(0)}$3d3/2. Additionally, 78% of the precursor Pd^{2+} ($PdCl_2$) ions in 1% Pd/graphene were reduced to $Pd^{(0)}$ [40]. Similarly, from the XPS spectrum of the 1% Cu/graphene catalyst (**Fig. 5i)**, the binding energies emerging at 952.56 eV and 932.70 eV corresponded to $Cu^{(0)}$2p1/2 and $Cu^{(0)}$2p3/2 [41]. Therefore, for 1% Cu/graphene, the reduction rate of the precursor $Cu(CH_3OO)_2 \cdot H_2O$ was 70.1%. According to the XPS spectrum of 1% Fe/graphene (**Fig. 5l**), the binding energies at 720.1 eV and 706.8 eV could be attributed to $Fe^{(0)}$2p1/2 and $Fe^{(0)}$2p3/2 [42], and the reduction degree of the precursor $FeCl_3 \cdot 6H_2O$ to $Fe^{(0)}$ was 85%. However, from the XPS spectrum of 1% Ru/graphene (**Fig. 5m and 5o**), the binding energies at 280.2, 462.0, and 484.1 eV corresponded to $Ru^{(0)}$3d5/2, $Ru^{(0)}$3p3/2, and $Ru^{(0)}$3p1/2 [39]. Additionally, the binding energies at 451.3 eV and 444.1 eV corresponded to $In^{(0)}$3d3/2 and $In^{(0)}$3d5/2 (**Fig. 5**) [43]. The reduction rate of precursor In ions was above 90%. Hence, the reduction rates of the precursor metal ions were in the range of 70–90%. Most of metals ions were reduced to $M^{(0)}$, which indicated that a successful preparation of the metal/graphene catalyst was achieved.

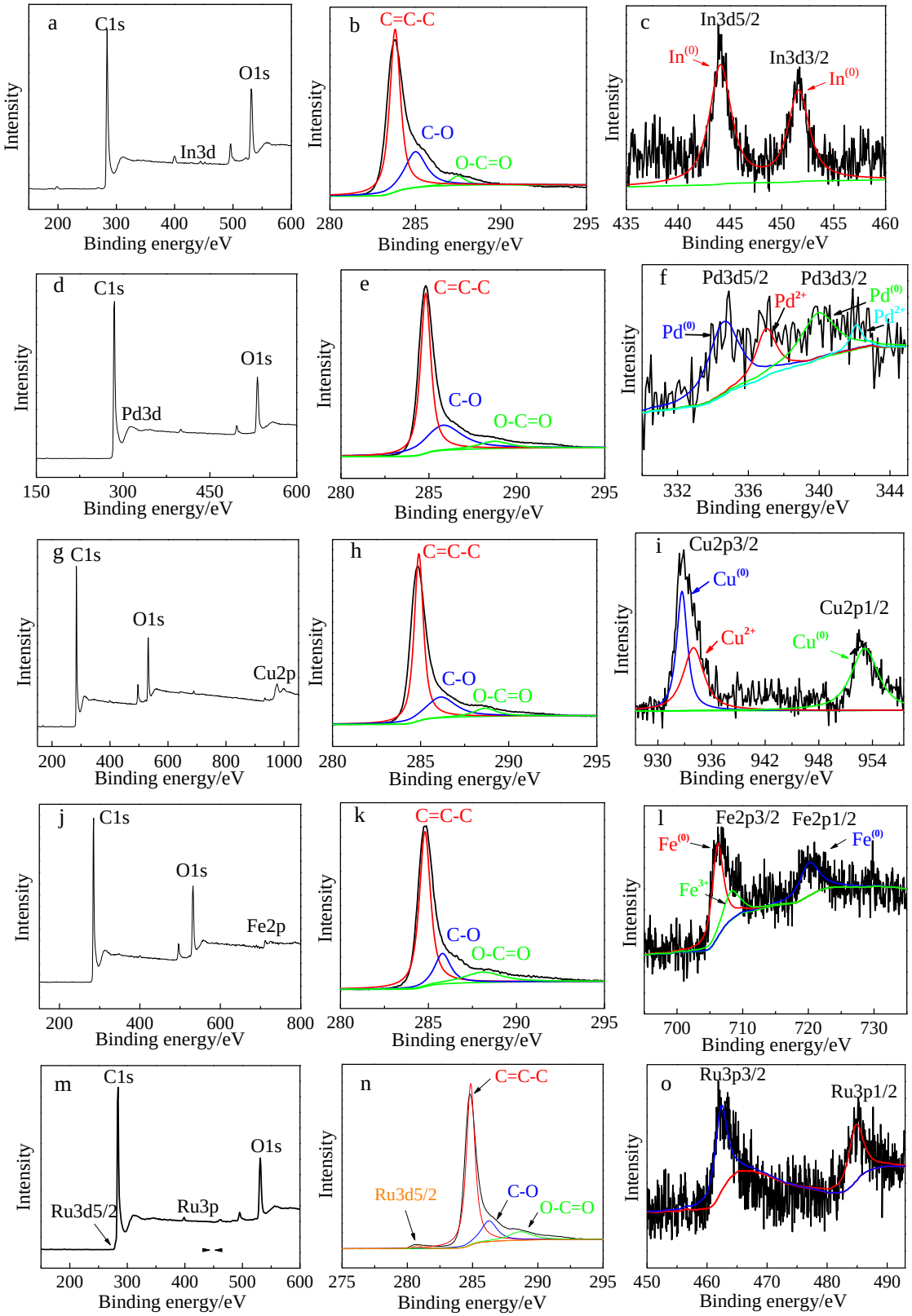

Figure 5. (a) Survey XPS spectrum, (b) C1s XPS spectrum, and (c) In3d XPS spectrum of 1%In/graphene catalyst; (d) Survey XPS spectrum, (e) C1s XPS spectrum, and (f) Pd3d XPS spectrum of 1%Pd/graphene catalyst; (g) Survey XPS spectrum, (h) C1s XPS spectrum, and (i) Cu2p XPS spectrum of 1%Cu/graphene catalyst; (j) Survey XPS spectrum, (k) C1s XPS spectrum, and (l) Fe2p XPS spectrum of 1%Fe/graphene catalyst; (m) Survey XPS spectrum, (n) C1s XPS spectrum, and (o) Ru3p XPS spectrum of 1%Ru/graphene catalyst.

The CO_2 electrochemical reduction properties were investigated on the prepared metal/graphene catalyst samples when the applied potentials were 0 to −2 V (vs. Ag|AgCl). In this study, an alkaline electrolyte solution of 0.5 mol/L $KHCO_3$ was used to promote the dissolution of CO_2, and there was an equilibrium reaction in the electrolyte solution [44]:

$$CO_{2(aq)}+H_2O \rightarrow HCO_3^-+H^+ \rightarrow CO_3^{2-}+2H^+ \quad (1)$$

Fig. 6a and **Fig. 7** show the CV scans of 1% In/graphene, 1% Pd/graphene, 1% Cu/graphene, 1% Fe/graphene, and 1% Ru/graphene catalysts at a scan rate of 200 mV/s in N_2-saturated and CO_2-saturated 0.5 mol/L $KHCO_3$. The reduction peak potentials for all metal/graphene catalysts and reduction currents at −2.0 V (vs. Ag|AgCl) are listed in **Table 1**.

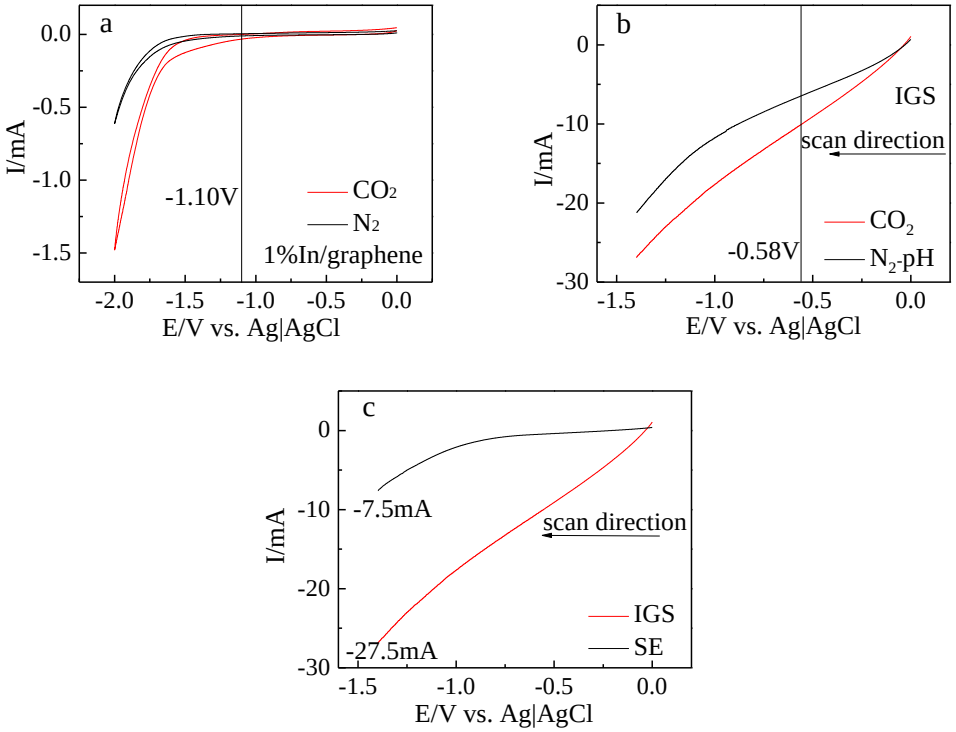

Figure 6. (a) CV scans at 200 mV/s in N_2-saturated and CO_2-saturated 0.5 mol/L $KHCO_3$ at glassy carbon electrode with 1%In/graphene; (b) LSV of IGS under CO_2 and N_2 at scan rate 100 mV/s; (c) LSV curve comparison of IGS and SE electrode under CO_2 at scan rate 100 mV/s.

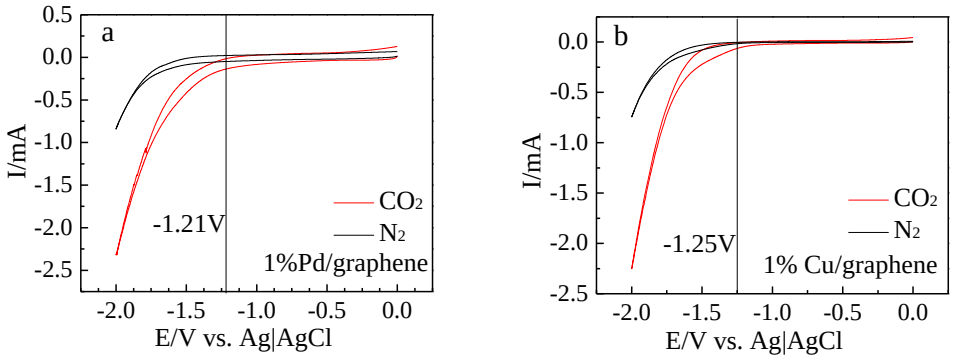

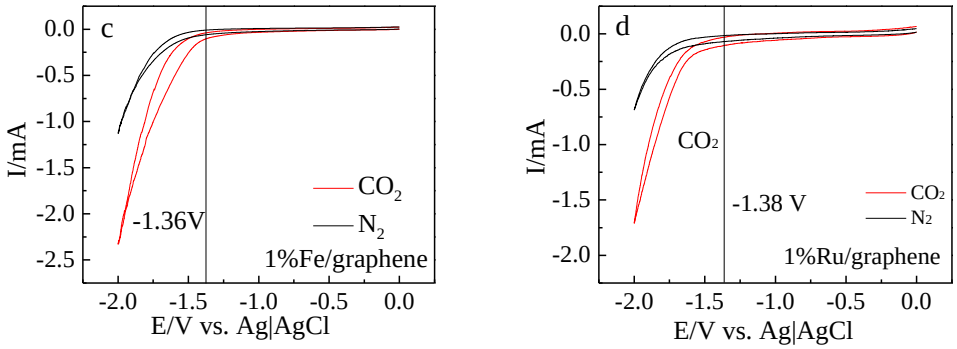

Figure 7. CV scans of GC electrode with (a) 1%Pd/graphene, (b) 1%Cu/graphene, (c) 1%Fe/graphene, and (d) 1%Ru/graphene catalysts at 200 mV/s in N_2-saturated and CO_2-saturated 0.5 mol/L $KHCO_3$.

As can be seen from the CV curves of the metal/graphene catalysts, when the voltage was less than the peak potential, sharp increases of the reduction current under CO_2, compared with the curves under N_2, could be observed, which was caused by the catalytic reduction of CO_2 (under CO_2). This indicated that all the metal/graphene catalysts exhibited a high catalytic activity for CO_2 reduction. However, the peak potential order was 1% In/graphene (−1.10 V) < 1% Pd/graphene (−1.21 V) < 1% Cu/graphene (−1.25 V) < 1% Fe/graphene (−1.36 V) < 1% Ru/graphene (−1.38 V). The potential E (vs. Ag|AgCl) can be converted to E (vs. SHE) in accordance with the formula (E^0 vs. SHE at 25 ºC and pH 7.0) [45]:

E (vs. SHE) = E (vs. Ag|AgCl) + 0.197 (2)

Peak potential was in the order of 1% In/graphene (−0.90 V) < 1% Pd/graphene (−1.01 V) < 1% Cu/graphene (−1.05 V) < 1% Fe/graphene (−1.16 V) < 1% Ru/graphene (−1.18 V). In 0.5 mol/L $KHCO_3$ saturated with CO_2, the CO_2 was adsorbed on the surface of the electrode material, $CO_{2(ads)}$ was then reduced to the free radical anion$\cdot CO_2^-{}_{(ads)}$. The intermediate product [H] of hydrogen evolution reaction (HER) was the key material for the reduction of $CO_{(ads)}$ to CH_4, C_2H_2 and so on. When electrodes had sufficient capacity for the adsorption of CO and hydrogen evolution was inhibited, then CO_2 would be reduced to CH_4 (Eq. (3)).

$CO_2 + 8H^+ + 8e^- \rightarrow CH_4 + 2H_2O$ $E^0 = -0.25$ V (3)

When the electrode rarely adsorbed CO, then stable radical anion adsorbed $CO_2^-{}_{(ads)}$ would not be formed and HCOOH became the main reduction product (Eq. (4)).

$CO_2 + 2H^+ + 2e^- \rightarrow HCOOH$ $E^0 = -0.61$V (4)

For the five metal (Pd, Fe, Cu, Ru, and In) samples, In had the highest hydrogen evolution potential and Pd had the lowest. The different adsorption capacities of the metal/graphene catalysts for CO caused the difference of the reduction peak potentials. The peak potentials of all metal/graphene catalysts were larger than the reaction potential of Eqs. (1)–(4). Both HCOOH and CH_4 could be the main products, which was related to the potential of HER and adsorption ability of the metal/graphene catalyst for CO.

3.2. Characterization and electrochemical test of MGS electrode

Graphene was prone to aggregate in solution because of its hydrophobic nature. Although the graphene surface was loaded with metal particles, it was still hydrophobic. With soft, flexible, macroporous, low-cost, and recyclable features, polyurethane and melamine sponges were both selected as the catalyst support materials. **Fig. 8** shows the SEM of PGS obtained with polyurethane and melamine sponges by three 'dipping and drying' processes. As shown in **Fig. 8b, 8d, 8f, and 8h**, no matter which preparation program was used, the resulting PGS (melamine sponge) was not ideal. Only minimal 1% Pd/graphene catalyst could be observed on the surface of the melamine sponge.

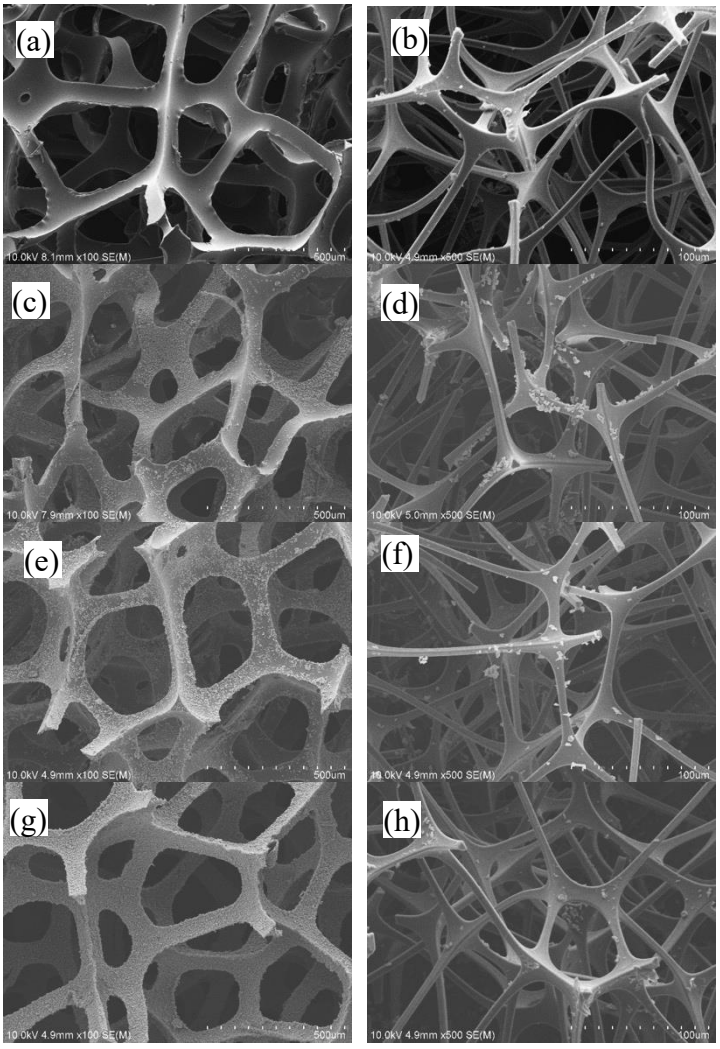

Figure 8. SEM pattern of (a) bare polyurethane sponge, (b) bare melamine sponge, (c) PGS (polyurethane sponge) fabricated with sodium holate, (d) PGS (melamine sponge) fabricated with sodium cholate, (e) PGS (polyurethane sponge) fabricated with sodium dodecyl benzene sulfonate, (f) PGS (melamine sponge) fabricated with sodium dodecyl benzene sulfonate, (g) PGS (polyurethane sponge) fabricated with C_2H_5OH, and (h) PGS (melamine sponge) fabricated with C_2H_5OH.

For a polyurethane sponge, the 1% Pd/graphene catalyst was well supported on the surface when ethanol was used as solvent without addition of a surfactant (shown in **Fig. 8a and 8g**).

Owing to the mechanical flexibility of the 1% Pd/graphene catalyst and strong van der Waals interactions [46] between the polyurethane sponge and 1% Pd/graphene catalyst, 1% Pd/graphene catalyst were physically coated onto the polyurethane sponge skeletons.

The SEM patterns of 1% Cu/graphene/polyurethane sponge (CGS), 1% Fe/graphene/polyurethane sponge (FGS), 1% In/graphene/polyurethane sponge (IGS), and 1% Ru/graphene/polyurethane sponge (RGS) electrodes, prepared by the same method, are shown in **Fig. 9**. The metal/graphene catalysts were well dispersed on the surface of the polyurethane sponge. In these samples, electron transfer could be achieved efficiently and the morphology and open porous structure of the polyurethane sponge were not changed compared with the original state. The metal/graphene catalyst coatings created an electrically conductive surface on the polyurethane sponge, which provided a channel for electron transfer during the catalytic reduction of CO_2. Additionally, a stainless steel mesh (SS) was sandwiched between two pieces of polyurethane sponges to act as a current collector [32].

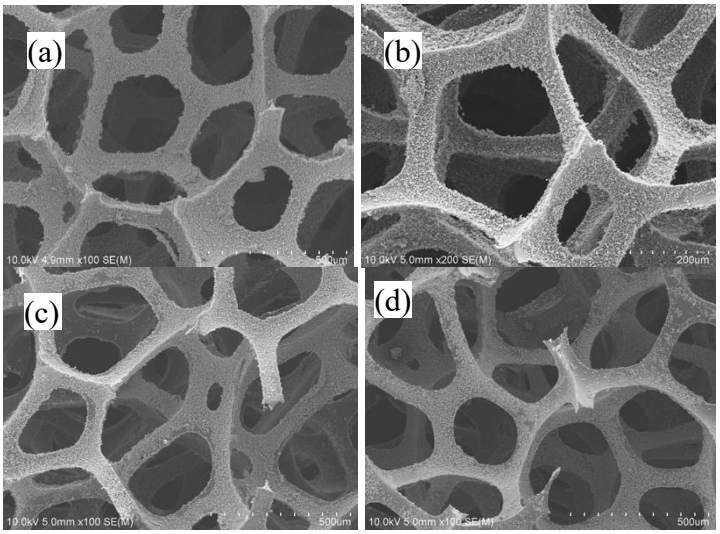

Figure 9. SEM pattern of (a) CGS (polyurethane sponge) fabricated with ethanol, (b) FGS (polyurethane sponge), (c) IGS (polyurethane sponge), and RGS (polyurethane sponge) fabricated with C_2H_5OH.

The electrochemical properties of the MGS electrode were characterized by LSV. The pH of 0.5 mol/L $KHCO_3$ saturated with CO_2 decreased, owing to the reaction:

$$CO_2 + H_2O \rightarrow HCO_3^- + H^+ \quad (5)$$

However, CO_2 in 0.5 mol/L $KHCO_3$ was removed when the electrolyte solution was saturated with N_2, which led to an increase of the pH. The pH of N_2-saturated 0.5 mol/L $KHCO_3$ was 9.45, but CO_2-saturated 0.5 mol/L $KHCO_3$ was 7.60. The pH value will affect the electrode potentials for the reduction of H_2O and CO_2 in accordance with the Eqs (1), (3), (4), and (6).

$$2H^+ + 2e^- \rightarrow H_2 \quad E^0 = -0.41 \text{ V} \quad (6)$$

The LSV curve comparison of MGS prepared at different scan speeds under CO_2 or N_2 is shown in **Fig. 10**. The reduction current increased with the scanning speed.

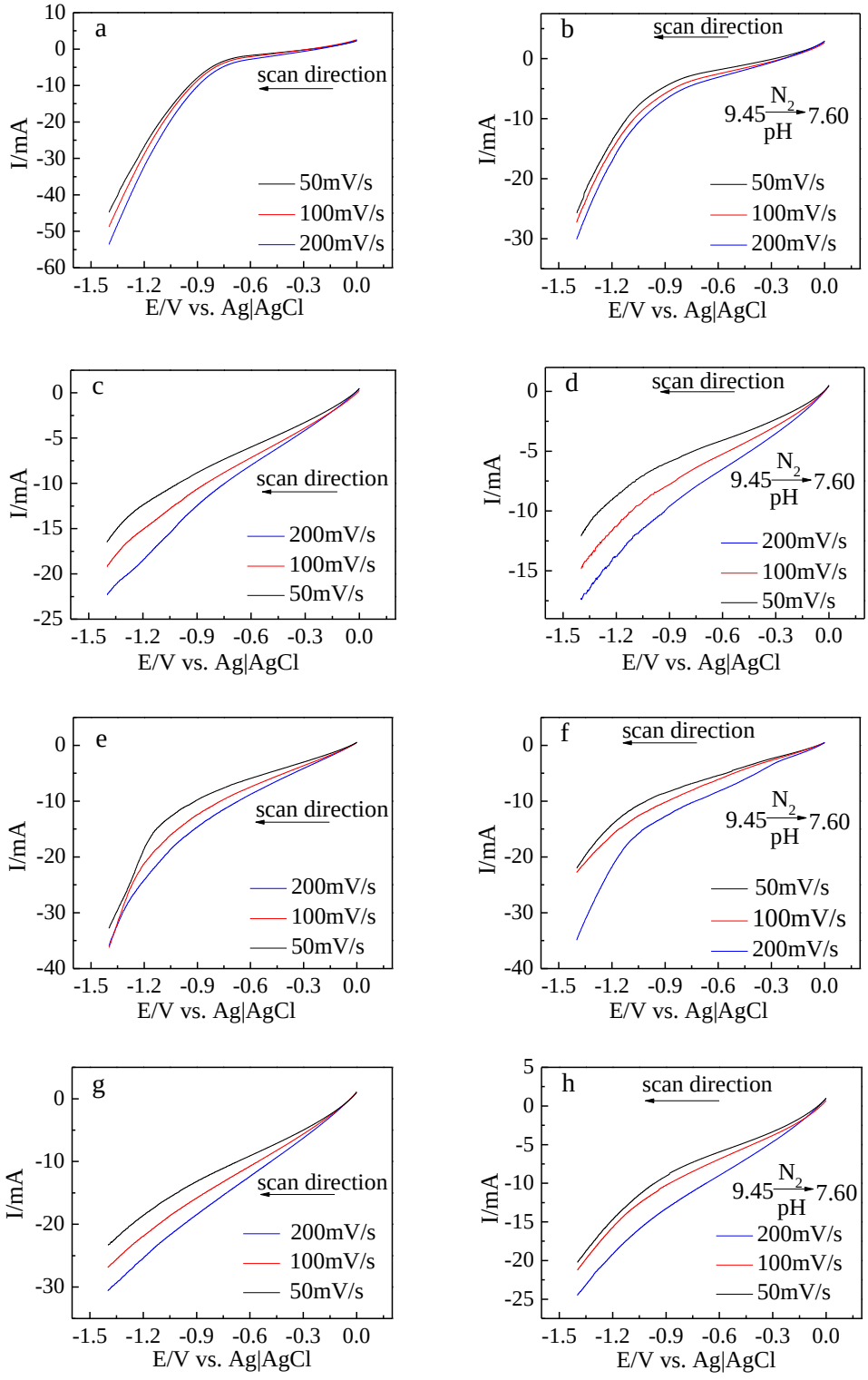
a
scan direction
50mV/s
100mV/s
200mV/s
I/mA
E/V vs. Ag|AgCl
b
scan direction
9.45 N2 7.60
pH
50mV/s
100mV/s
200mV/s
I/mA
E/V vs. Ag|AgCl
c
scan direction
200mV/s
100mV/s
50mV/s
I/mA
E/V vs. Ag|AgCl
d
scan direction
9.45 N2 7.60
pH
200mV/s
100mV/s
50mV/s
I/mA
E/V vs. Ag|AgCl
e
scan direction
200mV/s
100mV/s
50mV/s
I/mA
E/V vs. Ag|AgCl
f
scan direction
9.45 N2 7.60
pH
50mV/s
100mV/s
200mV/s
I/mA
E/V vs. Ag|AgCl
g
scan direction
200mV/s
100mV/s
50mV/s
I/mA
E/V vs. Ag|AgCl
h
scan direction
9.45 N2 7.60
pH
200mV/s
100mV/s
50mV/s
I/mA
E/V vs. Ag|AgCl

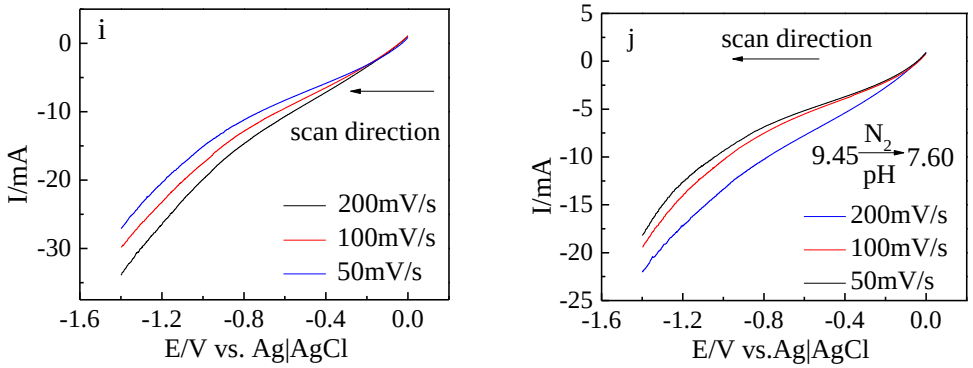

Figure 10. LSV of PGS electrode under (a) CO_2, (b) N_2; LSV of CGS under (c) CO_2, (d) N_2; LSV of FGS under (e) CO_2, (f) N_2; LSV of IGS under (g) CO_2, (h) N_2; LSV of RGS under (i) CO_2, (j) N_2.

As shown in **Fig. 6b** and **Fig. 11**, LSV scans of the PGS, CGS, FGS, IGS and RGS electrodes under CO_2 and N_2 at a scan rate of 100 mV/s were carried out. For PGS, when the potential was lower than −0.78 V, the reduction current under CO_2 was higher than that under N_2. This indicated that CO_2 in the electrolyte was captured strongly by the PGS GDE and catalytically reduced.

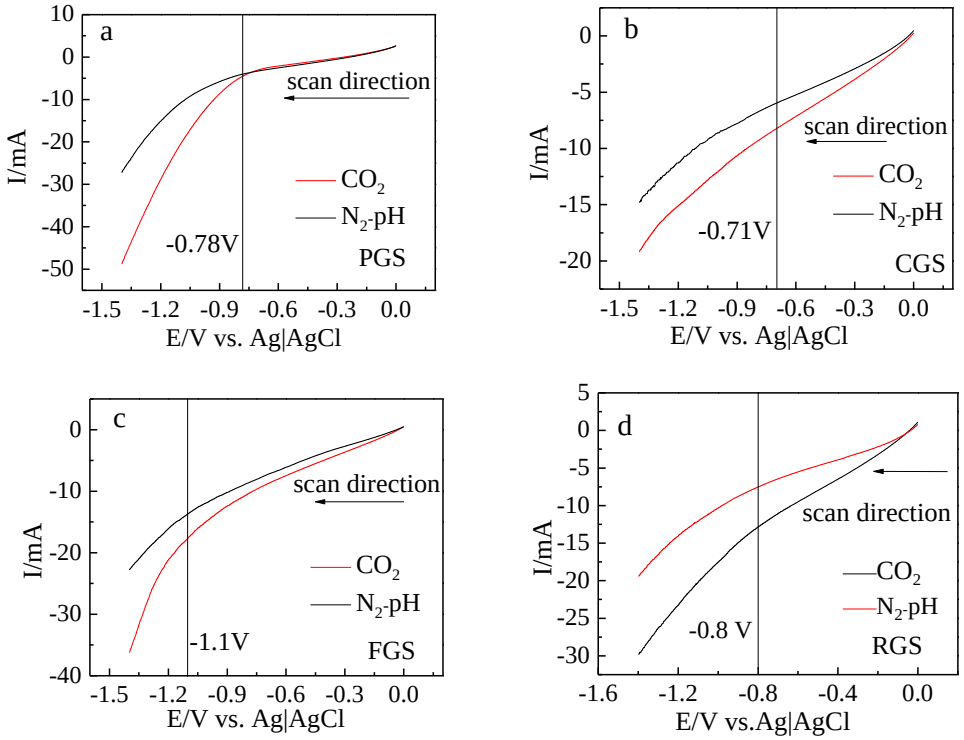

Figure 11. LSV of (a) PGS, (b) CGS, (c) FGS and (d) RGS electrode under CO_2 and N_2 at scan rate 100 mV/s.

The peak potentials of CGS, FGS, IGS, and RGS were −0.71 V, −1.1 V, −0.58 V, and −0.8 V, respectively. The peak potential of IGS was most positive compared with the other three catalyst

samples, which was consistent with previous results. For GDE, not only did the hydrogen evolution potential of the catalyst and the adsorption capacity of CO influence the reduction peak potential, but also the coverage of metal/graphene catalyst on the sponge and the ability to capture CO_2 played a vital role.

The LSV curve comparison of MGS (PGS, CGS, FGS, RGS, and IGS) and polyurethane sponge electrode (SE) at a scan rate 100 mV/s under CO_2 is shown in **Fig. 12** and **Fig. 6c,** respectively. The reduction current of MGS at −1.4 V is listed in **Table 1** and decreased in the order of PGS > FGS > RGS > IGS > CGS (49.1 mA > 37.5 mA > 29.1 mA > 27.5 mA > 18.1 mA). However, the reduction current of SE was only 7.5 mA. By comparing the LSV curve of MGS and SE, the current value of the no-load electrode (SE) was found to be much lower than that of the loading electrode (MGS). The polyurethane sponge was not conductive, so an electron transport channel should be provided by the metal/graphene catalysts covered on the surface of the sponge. The catalytic ability and coverage of metal/graphene on the polyurethane sponge would be related with the reduction current. From the comparison of the SEM of MGS, the coverage of PGS was the best, and the reduction current was the highest. Furthermore, the CO_2 reduction reaction and the HER were promoted. However, because of the porous nature of the sponge electrode, a large amount of CO_2 was captured and the CO_2 local concentration on the electrode surface was higher than that in the solution. Hence, the catalytic reduction reaction of CO_2 was further improved using MGS.

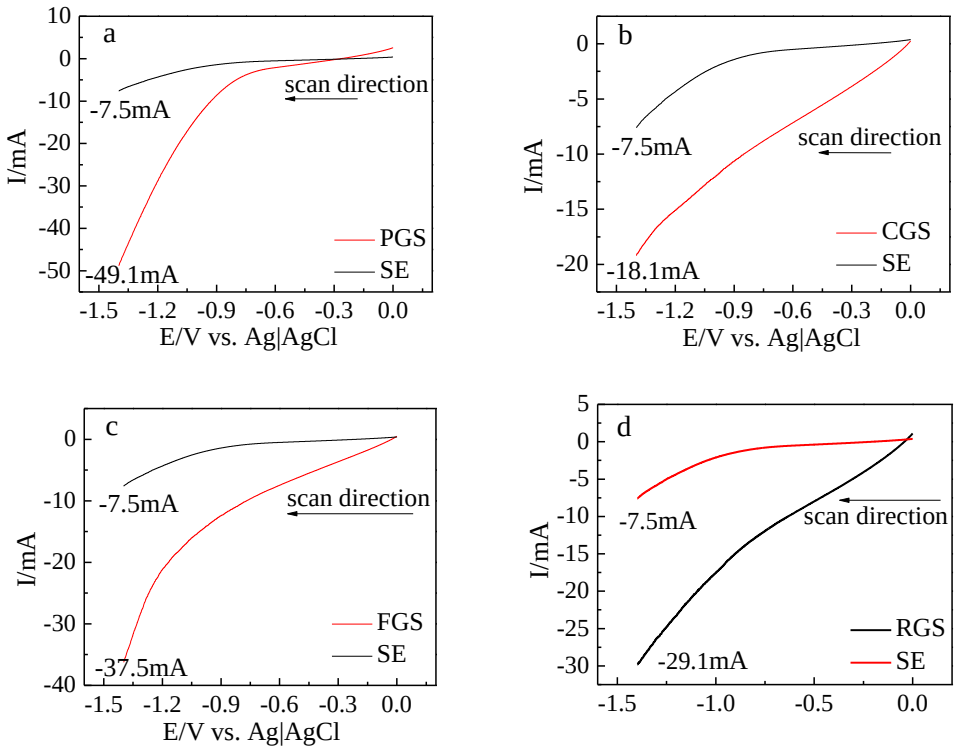

Figure 12. LSV curve comparison of (a) PGS and SE electrode, (b) CGS and SE electrode, (c) FGS and SE electrode, and (d) RGS and SE electrode under CO_2 at scan rate 100 mV/s.

It is worth noting that the onset overpotential for IGS was more positive and formate could be detected on IGS with a Faradaic efficiency of 71.9%. A comparison between our results and those obtained for some representative recently studied catalyst systems is given in Table 2. The catalytic performance of the present IGS was better than most of those reported.

Table 2. Comparison of some representative studies conducted in recent years for the electrochemical reduction of CO_2 to formate or formic acid

Electrocatalyst	Peak potential (Ag|AgCl)	Max. FE of HCOOH	Electrolyte	Ref.
Cu nanofoam	-1.1 V	37%	0.1 mol/L $KHCO_3$	[47]
P-SGDE	-1.4 V	70%	0.5 mol/L $KHCO_3$	[48]
3D Skeleton (sponge) Cu	-1.1 V	34%	0.5 mol/L $NaHCO_3$	[49]
N-graphene	-1.1 V	71%	0.5 mol/L $KHCO_3$	[50]
IGS	-0.58 V	71.9%	0.5 mol/L $KHCO_3$	This work

4. CONCLUSIONS

Mono-metal (Pd, Fe, Cu, Ru, and In)/graphene/polyurethane sponge catalysts were prepared and fully characterized using XRD, XPS, SEM, and TEM. The relative contents of graphitic carbon in metal/graphene were estimated, and were in the order of 1% Pd/graphene (60.1%) < 1% Cu/graphene (65.5%) < 1% Fe/graphene (65.8%) < 1% Ru/graphene (66.7%) < 1% In/graphene (67.1%). Suitable contents of remaining oxygen groups and sp^2 carbons played an important role in the construction of the metal/graphene catalysts. Pd, Cu, Fe, Ru, and In nanoparticles were successfully loaded and uniformly dispersed on the graphene surface. The reduction degree of the metal predecessor to $M^{(0)}$ was approximately 80%. Electrocatalytic reduction properties of the prepared catalysts were evaluated by the CV curve. The reduction peak potentials were in the order of 1% In/graphene (−1.10 V) < 1% Pd/graphene (−1.21 V) < 1% Cu/graphene (−1.25 V) < 1% Fe/graphene (−1.36 V) < 1% Ru/graphene (−1.38 V). From the SEM of MGS, the coverage of 1% Pd/graphene was the best, and the reduction current (49.1 mA) was far higher than that of SE (7.5 mA) at −1.4 V. The coverage of metal/graphene severely affected the current. So the metal/graphene on the polyurethane sponge improved the electrical conductivity of MGS. However, the reduction peak potential order of MGS was consistent with GC as 1% In/graphene (−0.58 V) < 1% Cu/graphene (−0.71 V) < 1% Pd/graphene (−0.78 V) < 1% Ru/graphene (−0.8 V) < 1% Fe/graphene (−1.1 V). The hierarchical macroporous, high internal surface and junction free network structure guaranteed access of the electrolyte to the surface of the MGS electrode. From the electrochemical test, the MGS electrode could capture CO_2 and resulted in a higher CO_2 concentration on their surface than that in solution, which promoted their excellent catalytic properties for the CO_2 reduction.

ACKNOWLEDGEMENTS
Authors gratefully acknowledge financial support from Major Science and Technology Program for Water Pollution Control and Treatment, China (No. 2018ZX07101005), the National Natural Science Foundation of China (No. 21872009), Beijing Natural Science Foundation, China (Z170004), and National Key R&D Program of China (No. 2018YFC1802500).

References

1. R. Zhang, W.X. Lv and L.X. Lei, *Appl. Surf. Sci.*, 356 (2015) 24.
2. B.H. Zhang, Z.H. Guo, Z. Zuo, W. Pan and J.T. Zhang, *Appl. Catal., B,* 239 (2018) 441.
3. G.X. Song, F. Xin and X.H. Yin, *J. Colloid Interface Sci.*, 442 (2015) 60.
4. M.F. Ehsan and T. He, *Appl. Catal., B,* 166 (2015) 345.
5. X.C. Kang, Q.G, Zhu, X.F. Sun, J.Y. Hu, J.L. Zhang, Z.M. Liu and B.X. Han, *Chem. Sci.*, 7 (2016) 266.
6. Z.G. Zhang, Z.F. Huang, X.D. Cheng, Q.L. Wang, Y. Chen, P.M. Dong and X.W. Zhang, *Appl. Surf. Sci.*, 355 (2015) 45.
7. J.H. Kim, H. Woo, S.W. Yun, H.W. Jung, S. Back, Y. Jung and Y.T. Kim, *Appl. Catal., B,* 213 (2017) 211.
8. J.L. White and A.B. Bocarsly, *J. Electrochem. Soc.*, 163 (2016) H410.
9. E.A. Batista and M.L.A. Temperini, *J. Electroanal. Chem.*, 629 (2009) 158.
10. R. Kortlever, C. Balemans, Y. Kwon and M.T.M. Koper, *Catal. Today,* 244 (2015) 58.
11. Y.Z. Zhu, Z.X. Xu, Q.Q. Lang, W.Y. Jiang, Q.Q. Yin, S.X. Zhong and S. Bai, *Appl. Catal., B,* 206 (2017) 282.
12. Q. Zhang, W.T. Xu, J. Xu, Y.Y. Liu and J.J. Zhang, *Catal. Today*, 318 (2018) 15.
13. H. Xie, T.Y. Wang, J.S. Liang, Q. Li and S.H. Sun, *Nano Today,* 21 (2018) 41.
14. H.J. Hu, Y. Tang, Q. Hu, P.Y. Wan, L.M. Dai and X.J. Yang, *Appl. Surf. Sci.*, 445 (2018) 281.
15. D. Plana, J. Florez-Montano, V. Celorrio, E. Pastor and D.J. Fermin, *Chem. Commun.*, 49 (2013) 10962.
16. G.H. Jin, C.G. Werncke, Y. Escudiee, S. Sabo-Etienne and S. Bontemps, *J. Am. Chem. Soc.*, 137 (2015) 9563.
17. H.A. Hansen, J.B. Varley, A.A. Peterson and J.K. Norskov, *J. Phys. Chem. Lett.*, 4 (2013) 388.
18. B. Eneau-Innocent, D. Pasquier, F. Ropital, J.M. Leger and K.B. Kokoh, *Appl. Catal., B,* 98 (2010) 65.
19. H. De Jesus-Cardona, C. del Moral and C.R. Cabrera, *J. Electroanal. Chem.*, 513 (2001) 45.
20. V. Tripkovic, M. Vanin, M. Karamad, M.E. Bjorketun, K.W. Jacobsen, K.S. Thygesen and J. Rossmeisl, *J. Phys. Chem. C*, 117 (2013) 9187.
21. C. Genovese, C. Ampelli, S. Perathoner and G. Centi, *J. Energ. Chem.*, 22 (2013) 202.
22. G.Q. Zhang, Z. Li, H.Y. Zheng, T.J. Fu, Y.B. Ju and Y.C. Wang, *Appl. Catal., B,* 179 (2015) 95.
23. X.Q. An, K.F. Li and J.W. Tang, *ChemSusChem*, 7 (2014) 1086.
24. H.J. Li, Z.W. Xu, K.Z. Li, X.H. Hou, G.X. Cao, Q.L. Zhang and Z.Y. Cao, *J. Mater. Chem.*, 21 (2011) 1181.
25. L.Q. Jiang, M. Li, L. Lin, Y.F. Li, X.Q. He and L.L. Cui, *RSC Adv.* 4 (2014) 26653.
26. T.W. Ebbesen, H.J. Lezec, H. Hiura, J.W. Bennett, H.F. Ghaemi and T. Thio, *Nature* 382 (1996) 54.
27. D.H. Lim, J.H. Jo, D.Y. Shin, J. Wilcox, H.C. Ham and S.W. Nam, *Nanoscale*, 6 (2014) 5087.
28. R.L. Machunda, H. Ju and J. Lee, *Curr. Appl. Phys.* 11 (2011) 986.
29. H. Wang and J.L. Wang, *Electrochim. Acta*, 53 (2008) 6402.
30. J. Ge, H.B. Yao, W. Hu, X.F. Yu, Y.X. Yan, L.B. Mao, H.H. Li, S.S. Li and S.H. Yu, *Nano Energy*, 2 (2013) 505.
31. W. Chen, R.B. Rakhi, L.B. Hu, X. Xie, Y. Cui and H.N. Alshareef, *Nano Lett.* 11 (2011) 5165.
32. X. Xie, G.H. Yu, N. Liu, Z.N. Bao, C.S. Criddle and Y. Cui, *Energ. Environ. Sci.* 5 (2012) 6862.
33. W.S. Hummers Jr and R.E. Offeman, *J. Am. Chem. Soc.*, 80 (1958) 1339.
34. L.J. Cote, F. Kim and J.X. Huang, *J. Am. Chem. Soc.*, 131 (2009) 1043.
35. X. Liu, L.S. Zhu, H. Wang, G.Y. He and Z.Y. Bian, *RSC Adv.* 6 (2016) 38380.
36. W.Z. Li, C.H. Liang, W.J. Zhou, J.S. Qiu, Z.H. Zhou, G.Q. Sun and Q. Xin, *J. Phys. Chem. B,* 107 (2003) 6292.

37. G.Y. Gao, D.J. Guo and H.L. Li, *J. Power Sources*, 162 (2006) 1094.
38. M. Zawadzki and J. Okal, *Cata. Today*, 257 (2015) 136.
39. J. Okal, M. Zawadzki and W. Tylus, *Appl. Catal., B*, 101 (2011) 548.
40. P. Matczak and S. Romanowski, *Cent. Eur. J. Chem.*, 9 (2011) 474.
41. L. Lianos, Y. Debauge, J. Massardier, Y. Jugnet and J.C. Bertolini, *Cata. Lett.*, 44 (1997) 211.
42. W.P. Yang, D. Costa and P. Marcus, *J. Electrochem. Soc.*, 141 (1994) 2669.
43. N.L. Shruthi, K.G. Deepa, M.A. Sunil and J. Nagaraju, *Appl. Surf. Sci.*, 316 (2014) 424.
44. W.X. Lv, R. Zhang, P.R. Gao and L.X. Lei, *J. Power Sources*, 253 (2014) 276.
45. R.P.S. Chaplin and A.A. Wragg, *J. Appl. Electrochem.*, 33 (2003) 1107.
46. D.D. Nguyen, N.H. Tai, S.B. Lee and W.S. Kuo, *Energ. Environ. Sci.,* 5 (2012) 7908.
47. S. Sen, D. Liu and G.T.R. Palmore, *ACS Catal.*, 4 (2014) 3091.
48. Q.N. Wang, H. Dong, H. Yu and H.B. Yu, *J. Power Sources,* 279 (2015) 1.
49. A. Dutta, M. Rahaman, M. Mohos, A. Zenetti and P. Broekmann, *ACS Catal.,* 7 (2017) 5431.
50. H.X. Wang, Y.B. Chen, X.L. Hou, C.Y. Ma and T.W. Tan, *Green Chem.,* 18 (2016) 3250.